

Article

Facile Low Temperature Hydrothermal Synthesis of BaTiO₃ Nanoparticles Studied by In Situ X-ray Diffraction

Ola G. Grendal ¹, Anders B. Blichfeld ¹ , Susanne L. Skjærø ¹ , Wouter van Beek ²,
Sverre M. Selbach ¹, Tor Grande ¹ and Mari-Ann Einarsrud ^{1,*} 

¹ Department of Materials Science and Engineering, NTNU Norwegian University of Science and Technology, 7491 Trondheim, Norway; ola.g.grendal@ntnu.no (O.G.G.); anders.b.blichfeld@ntnu.no (A.B.B.); susanne.l.skjarvo@ntnu.no (S.L.S.); sverre.magnus.selbach@ntnu.no (S.M.S.); tor.grande@ntnu.no (T.G.)

² Swiss-Norwegian Beamlines at European Synchrotron Research Facility, 38043 Grenoble, France; wouter@esrf.fr

* Correspondence: mari-ann.einarsrud@ntnu.no; Tel.: +47-735-94-002

Received: 30 April 2018; Accepted: 15 June 2018; Published: 17 June 2018



Abstract: Ferroelectric materials are crucial for today's technological society and nanostructured ferroelectric materials are important for the downscaling of devices. Controlled and reproducible synthesis of these materials are, therefore, of immense importance. Hydrothermal synthesis is a well-established synthesis route, with a large parameter space for optimization, but a better understanding of nucleation and growth mechanisms is needed for full utilization and control. Here we use in situ X-ray diffraction to follow the nucleation and growth of BaTiO₃ formed by hydrothermal synthesis using two different titanium precursors, an amorphous titania precipitate slurry and a Ti-citric acid complex solution. Sequential Rietveld refinement was used to extract the time dependency of lattice parameters, crystallite size, strain, and atomic displacement parameters. Phase pure BaTiO₃ nanoparticles, 10–15 nm in size, were successfully synthesized at different temperatures (100, 125, and 150 °C) from both precursors after reaction times, ranging from a few seconds to several hours. The two precursors resulted in phase pure BaTiO₃ with similar final crystallite size. Finally, two different growth mechanisms were revealed, where the effect of surfactants present during hydrothermal synthesis is discussed as one of the key parameters.

Keywords: BaTiO₃; hydrothermal synthesis; in situ; X-ray diffraction; nanoparticles

1. Introduction

Nanostructured ferroelectric materials are central for further development of electronics and information technology [1]. To answer this demand, cheap, controllable, scalable, environmentally friendly, simple, and reproducible fabrication routes must be developed. Wet chemical methods [2], like hydrothermal syntheses, are among the most promising routes [3].

BaTiO₃ (BT) has been of technological interest for many years due to its ferroelectric properties below 125 °C (non-volatile ferroelectric memories), piezo- and pyroelectricity (sonar, detectors, bone implants), and high dielectric constant and low dielectric loss (capacitors, thermistors, transducers) [4]. A variety of precursors and solvents have been shown to yield BT under various hydrothermal conditions [5]. Different sizes and morphologies have been reported, including spherical nanoparticles [6], -rods [7], and -cubes [8]. Dutta and Gregg [9] reported a hydrothermal synthesis, giving 0.2–1 µm sized BT particles after reaction times of 24 h or longer. Precursors used were TiO₂ (anatase) particles and BaCl₂ or Ba(OH)₂ in water with NaOH as a mineralizer. The synthesized BT

particles were reported to be larger, with a larger tetragonality and a more faceted morphology using BaCl_2 as Ba-source compared with Ba(OH)_2 . Cai et al. [8] described a synthesis using $\text{Ba(NO}_3)_2$ and titanium (IV) *n*-butoxide in a water-1-butanol mixture with KOH as a mineralizer. Reactions at 135 °C for 16 h gave cube-like BT particles, with a size of around 10 nm. The size of the nanoparticles could be controlled by the Ba:Ti ratio in the precursor solution. Li et al. [10] used BaCl_2 and TiCl_4 in a water-ethanol mixture with KOH as a mineralizer and obtained spherical BT nanoparticles after reactions at 230 °C for 12 h.

Obtaining insight into the nucleation and growth mechanism of the nanoparticles will facilitate control of the size and morphology of the final product, which is of great importance for the full utilization of the hydrothermal method. A few works have focused on describing the nucleation and growth mechanisms of BT from hydrothermal synthesis, often using the Johnson-Mehl-Avrami equation [11]:

$$f = 1 - \exp(-k(t - t_0)^n) \quad (1)$$

Here, f is the fractional extent of the reaction as a function of time (t) after the first appearance of the phase (t_0), k is a rate constant, and n is an exponent linked to the growth mechanism [11]. This model is derived for solid state reactions, but have also been successfully used for hydrothermal growth [12–14]. Ex situ studies are most often employed, where the reaction is quenched at various reaction times. Hertl [15] studied the hydrothermal reaction between TiO_2 and Ba(OH)_2 , and suggested that the rate limiting factor was a topochemical reaction of Ba^{2+} with TiO_2 at the surface of TiO_2 , with an activation energy of 105.5 kJ/mol. Similar conditions were investigated by Eckert et al. [16], who suggested two growth regimes: A dissolution-precipitation mechanism at the early stage and in situ transformation at a later stage. A limited number of data points makes it challenging to draw such conclusions as an initial nucleation and growth mechanism could occur before the dissolution-precipitation step [16]. Özen et al. [17] studied the formation of BT from a peroxo-hydroxide precursor (single source precursor for BT) in a NaOH solution. A clear change in the rate limiting step was reported as a function of temperature, but few data points make it challenging to deduce the mechanism. Still, a dissolution-precipitation mechanism was proposed. An increased reaction rate was observed with increasing temperature and an activation energy of 43.2 kJ/mol was reported.

The challenge in finding the growth mechanism from few data points and possible side effects of quenching can be overcome by following the reactions in real time through in situ experiments at synchrotron or neutron facilities. However, only a limited number of in situ studies of hydrothermal synthesis have been reported [18–20], with only two focusing on BT [21,22]. Walton et al. [21] followed the reaction between anatase and Ba(OD)_2 in D_2O by in situ neutron scattering. Here, a dissolution-precipitation mechanism was found as the rate limiting step, with an activation energy of 55 kJ/mol. Philippot et al. [22] used in situ X-ray diffraction to study the formation of BT from barium (II)- and titanium (IV)-isopropoxide in a water-ethanol mixture, with a time resolution of 5 s. Two growth regimes were suggested for the BT nanoparticles, an initial nucleation and growth limited mechanism with a high growth rate, followed by a dissolution-precipitation mechanism with a lower growth rate.

In this work, we present, for the first time, an in situ synchrotron X-ray diffraction study of a facile *aqueous* hydrothermal synthesis route to nanostructured BT using two different precursors, an amorphous titania precipitate slurry and a Ti-citric acid complex solution. Diffraction data with a time resolution down to 0.1 s at different temperatures (100, 125, and 150 °C) enabled the study of kinetics and growth in detail, demonstrating that the two precursors behave differently at low temperatures, but show similar characteristics at higher temperatures. From the amorphous titania precursor, nanocrystalline BT formed and stopped growing within 15 s at 150 °C, which, to the authors' knowledge, is the fastest that is reported in the literature for the hydrothermal synthesis of BT. Finally, the possible effect on the size and morphology of the nanoparticles by adding the surfactants, sodium dodecylbenzenesulfonate (SDBS) and ethylene glycol (EG), were investigated for the intermediate temperature.

2. Materials and Methods

2.1. Synthesis

The two different titanium precursors for the synthesis of the BT nanoparticles are described in the following. Titanium (IV) isopropoxide (TIP, Sigma-Aldrich, Oslo Norway, $\geq 97\%$) was mixed with distilled water under continuous stirring, forming a white amorphous Ti-OH precipitate with a Ti concentration of 0.3 M. Barium nitrate (Sigma-Aldrich, Oslo Norway, $\geq 99\%$), giving a 1:1 Ba:Ti-ratio, was then dissolved under continuous stirring, before the pH was raised to >14 by adding potassium hydroxide (KOH, Sigma-Aldrich, Oslo Norway, 80%). A slurry with a white precipitate was obtained. The KOH was mixed into the solution, while the solution was cooled in an ice-water bath. When used, both ethylene glycol (EG, Sigma-Aldrich, Oslo Norway, $>99\%$) and sodium dodecylbenzenesulfonate (SDBS, Sigma-Aldrich, Oslo Norway, technical grade) were added in a 1:1 mole ratio with Ti before KOH. Experiments from this route will be referred to as *Ti-slurry* (from the titanium slurry used as the titanium source) experiments.

For the other titanium precursor, TIP was dissolved in a 1.5 M citric acid solution (CA, Sigma-Aldrich, Oslo Norway, $\geq 99\%$) at 60 °C under continuous stirring, making a clear 0.43 M Ti complex solution. The pH was then increased from around 1, to pH = 5–6 by adding aqueous ammonia (Sigma-Aldrich, Oslo Norway, 25 wt % solution). Barium nitrate (Sigma-Aldrich, Oslo Norway, $\geq 99\%$), giving a 1:1 Ba:Ti-ratio, was then dissolved under continuous stirring, forming a clear solution. The pH was raised to >14 by adding potassium hydroxide (KOH, Sigma-Aldrich, Oslo Norway, 80%), resulting in the formation of a white precipitate. As for the Ti-slurry experiments, the surfactants, EG and SDBS, were included before KOH when used and in a 1:1 mole ratio with Ti. Experiments from this route will be referred to as *Ti-CAsol* (from the titanium-CA solution used as a titanium source) experiments. Approximately 5 mL of precursor was prepared for each experiment, for both the Ti-slurry and Ti-CAsol. An overview of the synthesis parameters for the experiments conducted in this work are presented in Table 1.

Table 1. Overview of sample names, temperature, pressure, X-ray wavelength, and time resolution for the in situ X-ray diffraction experiments. Also, indicated is the surfactants used for each experiment and the final product.

Name ^a	Temperature [°C]	Pressure [bar]	EG	SDBS	Wavelength ^b [Å]	Time Resolution ^c [s]	Final Product
Ti-slurry-100	100	200	no	no	0.7242	0.1	BT
Ti-slurry-125	125	200	no	no	0.7242	0.1	BT
Ti-slurry-150	150	200	no	no	0.7242	0.1	BT
Ti-slurry-EG	125	200	yes	no	0.7242	0.1	BT
Ti-slurry-SDBS	125	200	no	yes	0.7762	0.1	BT
Ti-CAsol-100	100	200	no	no	0.7129	10	BT + BC
Ti-CAsol-125	125	200	no	no	0.7129	5	BT
Ti-CAsol-150	150	200	no	no	0.7129	5	BT
Ti-CAsol-EG	125	200	yes	no	0.7242	5	BT + BC
Ti-CAsol-SDBS	125	200	no	yes	0.7129	5	BT

^a Ti-slurry and Ti-CAsol refers to the use of Ti-slurry and Ti-CAsol, respectively, for the titanium precursor.

^b Experiments conducted at different beam times, therefore, different wavelengths. ^c Time for collection of each 2D image file for the experiment. Exposure time was optimized for the different reaction speeds.

2.2. Characterization

The in situ X-ray diffraction experiments were performed at three different beam times using the Swiss-Norwegian Beamlines (BM01A) at the European Synchrotron and Radiation Facility (ESRF), Grenoble, France. The experiments were conducted in transmission mode, using the PILATUS@SNBL platform [23]. The experimental setup is described elsewhere [18,24,25]. In short, it consists of a single crystal sapphire capillary (1.15 ± 0.1 mm outer and 0.8 ± 0.08 mm inner diameter) that is pressurized with a high-pressure liquid chromatography (HPLC) pump and heated with a high temperature heat blower with nitrogen flow. The heat blower was heated to the desired set-point temperature and directed away from the capillary before being moved into position by a stepper motor. The set

point temperature was reached within 15 s. Heating profiles at selected temperatures are presented in Figure S1, with a description of the temperature calibration. The slurries were injected into the capillary quickly after preparation (1–2 min) to avoid BaCO_3 (BC) formation using a plastic syringe. All experiments were run until no changes were observed in the diffraction patterns (no change in intensity and/or peak width), varying from a few minutes to several hours.

All raw data frames were treated by masking parasitic regions (to remove shadow of beam stopper and diffraction spots from capillary) and integrated from 2D images to 1D diffractograms using *Bubble* (version 2017.10.23) [23]. The refinements were done using *TOPAS* (Bruker AXS version 5) in launch mode, with *jEdit* (version 4.3.1) as the text editor for writing macros for *TOPAS* [26]. The instrumental broadening was calibrated using a NIST 660a LaB_6 standard, fitted with the modified Thomson-Cox-Hastings pseudo-Voigt peak shape [27] and the “Simple Axial Model” supplied with *TOPAS*. For the refinements, zero error, scale factor, lattice parameter, Lorentzian isotropic size and strain parameter, isotropic thermal parameters for Ba and Ti, and a 25th order Chebyshev polynomial (to account for the broad background peak of water and solutes) were refined for each frame. The tetragonal unit cell of BT, being almost cubic, combined with the peak broadening from the nanosized BT made it impossible to differentiate between cubic and tetragonal space groups. The cubic space group (no. 221, $Pm\bar{3}m$) was, thus, chosen for describing BT in all experiments, using ICDD card #01-074-4539 as a reference.

3. Results

Typical color map plots for the Ti-slurry-150 and Ti-CAsol-150 experiments are presented in Figure 1a,b, respectively. For both experiments, BT forms directly from the amorphous precursor without intermediate phases and BT is the only phase appearing during the experiments. BT forms faster for the Ti-slurry (seconds) experiment than for the Ti-CAsol (minutes) experiment, which is a general trend for all reaction conditions and additives used.

The diffraction lines showed significant peak broadening, indicating nanosized crystallites. Anisotropic peak broadening and/or abnormal intensities were not observed, indicating nanosized spherical crystallites [25,28]. See Figure S2 for typical diffraction patterns and Rietveld refinements and Figure S3 for STEM images of Ti-CAsol-125 showing agglomerated spherical BT nanoparticles, with a size of <30 nm. A further discussion of the results using the two different precursors are provided in the following.

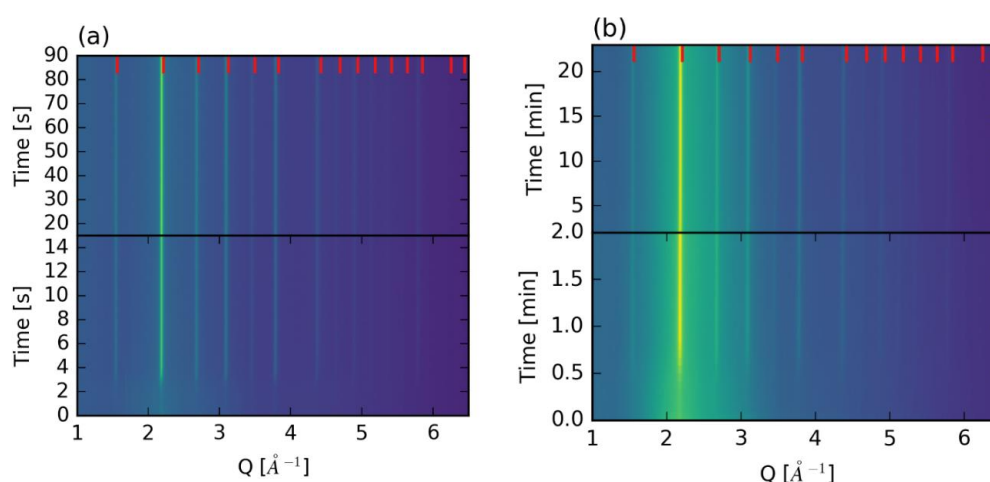


Figure 1. Color map plots showing the formation of BaTiO_3 at 150 °C and 200 bar (colors yellow-blue show intensity from high to low): (a) Ti-slurry-150 and (b) Ti-CAsol-150. Red markers show diffraction lines for bulk cubic BaTiO_3 at RT from ICDD card #01-074-4539, and the offset is an effect of temperature and finite-size effects. Notice the different time scales.

3.1. Ti-Slurry

Figure 2a–d shows the time resolved refined parameters for the Ti-slurry (scale factor, lattice parameter, crystallite size and strain) experiments at different temperatures. By increasing the reaction temperature, a small increase in the formation and growth rate is observed. The crystallite size stabilizes at around 15 nm after around 15 s at all three temperatures. The lattice parameter and strain are slightly decreasing, with an increasing reaction temperature from 4.0612(3) to 4.0587(2) Å and $1.27(7) \times 10^{-3}$ to $0.94(3) \times 10^{-3}$, respectively, when increasing the temperature from 100 to 150 °C.

Comparing the experiments with EG or SDBS as surfactants at 125 °C, there is no influence on the reaction rate. However, EG gives a small decrease in crystallite size (8.7(2) nm), while the presence of SDBS almost doubles the crystallite size (25.0(7) nm). The strain is similar for both EG and SDBS, but the decrease in strain is significantly slower for the Ti-slurry-EG. The lattice parameter for BT prepared in the Ti-slurry-EG is larger than for the Ti-slurry-SDBS, which can be directly linked to the size difference. The time resolved refined parameters (scale factor, lattice parameter, crystallite size and strain) for Ti-slurry-EG and Ti-slurry-SDBS are presented in Figure 2e–h.

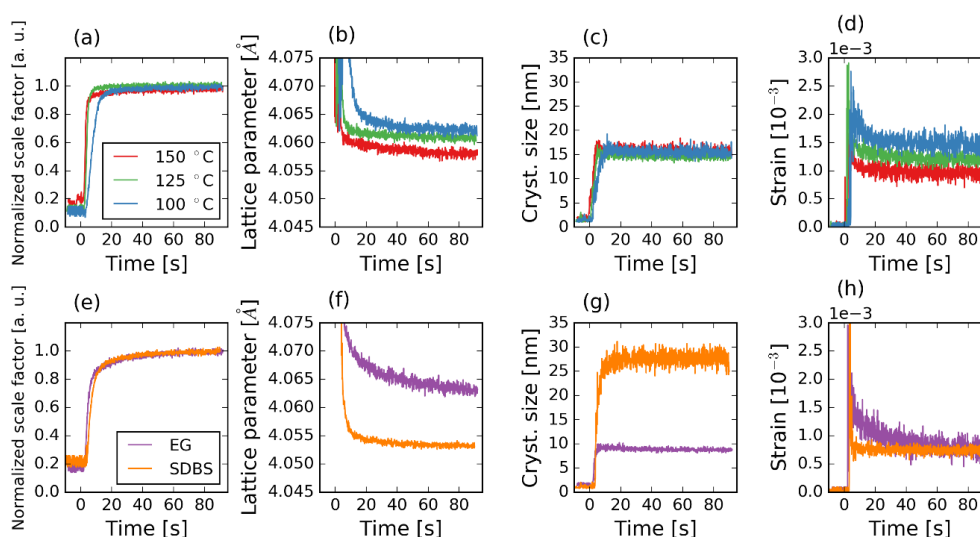


Figure 2. Time resolved refined values for the experiments with the Ti-slurry, showing scale factor (a,e), lattice parameter (b,f), crystallite size (c,g), and strain (d,h): (a–d) Ti-slurry-150, Ti-slurry-125, and Ti-slurry-100; (d–g) Ti-slurry-EG and Ti-slurry-SDBS at 125 °C. Scale factor is normalized to last value.

3.2. Ti-CAsol

The time resolved refined parameters (scale factor, lattice parameter, crystallite size, and strain) for the Ti-CAsol experiments at different temperatures are presented in Figure 3a–d. The three different temperatures yielded a significant difference in reaction rates, see scale factor in Figure 3a, where the amount of BT stabilized after 2, 10, and 200 min for reactions at 150, 125, and 100 °C, respectively. The final lattice parameter, crystallite size, and strain are not influenced significantly by the temperature, only the time for reaching the steady-state condition is influenced by temperature. The final values for Ti-CAsol-150 are 4.0502(2) Å, 12.5(2) nm, and $0.63(5) \times 10^{-3}$ for the lattice parameter, crystallite size, and strain, respectively (the final values for Ti-CAsol-100 and Ti-CAsol-125 are found in Table S1). The final values for the lattice parameter are smaller for the Ti-CAsol compared to the Ti-slurry.

The surfactant SDBS (at 125 °C) does not have a significant effect on the reaction rate or the final product, as can be seen by comparing Ti-CAsol-125 (Figure 3a–d) with Ti-CAsol-SDBS (Figure 3e–h). In the case of using EG, BC is formed before BT, effectively delaying the formation and growth of BT. The final parameters for the BT phase, in the case of Ti-CAsol-EG, are comparable to that of Ti-CAsol-125, as can be seen in Table S1.

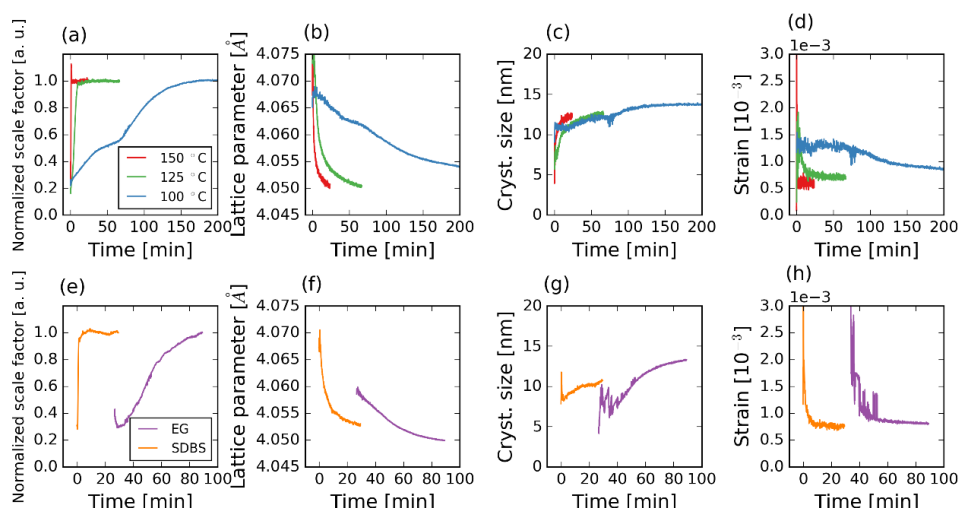


Figure 3. Time resolved refined values for the experiments with the Ti-CAsol, showing scale factor (a,e), lattice parameter (b,f), crystallite size (c,g), and strain (d,h): (a–d) Ti-CAsol-150, Ti-CAsol-125, and Ti-CAsol-100; (e–h) Ti-CAsol-EG and Ti-CAsol-SDBS at 125 °C. Scale factor is normalized to last value. Values for Ti-CAsol-EG are only plotted from around 20 min, since this is when BT formed.

3.3. Atomic Displacement Parameters

The isotropic Debye-Waller factor (B_{iso}) obtained from X-ray diffraction show the effect of the configurational static disorder and thermal vibration of atoms (dynamic disorder), and can give information about the ordering-disordering of a material [29]. The refined isotropic atomic displacement parameters for Ba and Ti (ADPs, B_{iso}) are presented in Figure 4a and b for Ti-slurry-150 and Ti-CAsol-150, respectively (ADPs for all experiments are presented in Figure S4, and Ti-CAsol-150 and Ti-slurry-150 are chosen here as representative examples). A fast reduction in the ADP for both Ba and Ti are observed at the early stage of the reaction, before the ADP stabilizes. This is a similar trend as is seen for the lattice parameter for both Ti-slurry-150 and Ti-CAsol-150. The ADP for Ti is higher than for Ba for both the Ti-slurry and Ti-CAsol experiments, which is consistent with similar works [22]. The main difference between Tisol-150 and Ti-CAsol-150 is the time scale, with Ti-slurry-150 showing a faster decrease and a shorter time for the ADPs to stabilize. The difference between the ADPs of Ti and Ba are smaller for the Ti-CAsol-150 than for Ti-slurry-150. A decrease in the final value for the ADP for Ti is observed with increasing temperature for both precursors. The opposite trend would be expected for a purely thermal effect, indicating less disordering, with increased reaction temperature. All refined values (scale factor, lattice parameter, size, strain, and B_{iso} for titanium and barium) for the last frame of all experiments are presented in Table S1.

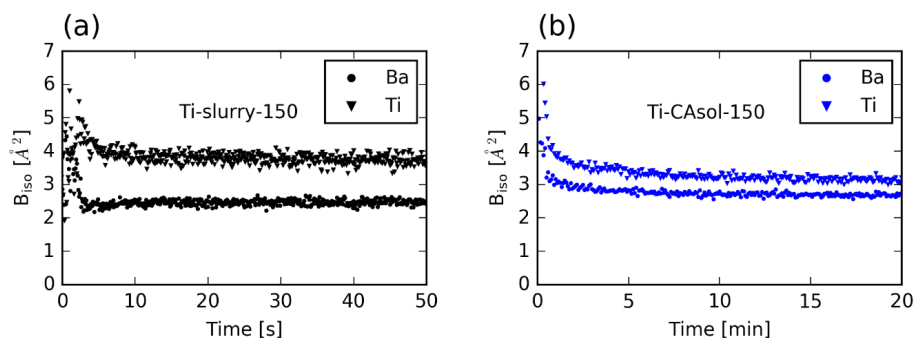


Figure 4. Isotropic atomic displacement parameters for Ba and Ti: (a) Ti-slurry-150 and (b) Ti-CAsol-150.

3.4. Kinetics of the Reactions

The scale factor of a phase is directly linked to the total amount of the corresponding phase. The scale factor can then be used to model the growth mechanism using Equation (1), with the normalized scale factor being the measure of the extent of the reaction [30]. Fits of Equation (1) to the scale factors are presented in Figure S5 and the refined values are summarized in Table 2. The Arrhenius plots for the Ti-slurry and Ti-CAsol experiments are presented in Figure 5a and the n -values from Equation (1) are plotted as a function of temperature in Figure 5b. The obtained activation energies are 22 and 41 kJ/mol for the Ti-CAsol and Ti-slurry, respectively (Table 2). The activation energy for the Ti-CAsol is approximately half that of the Ti-slurry, however, the uncertainty in the values is large.

The n -values for the Ti-slurry experiments fall into the same region for all temperatures (Figure 5b), showing a nucleation- and growth-controlled mechanism over the entire temperature range. The Ti-CAsol changes from a zero/first-order, or phase boundary-controlled mechanism, to a nucleation- and growth-controlled mechanism with increasing temperature.

Table 2. Fitted parameters for the growth of BT from in situ X-ray diffraction and the activation energy for the Ti-CAsol and Ti-slurry experiments.

Sample	k [s ⁻¹]	n ^a	R^2 [a.u.]	E_a [kJ/mol]
Ti-slurry-100	0.0130(6)	2.1	0.99	41
Ti-slurry-125	0.0126(6)	3.1	0.99	
Ti-slurry-150	0.063(5)	2.3	0.97	
Ti-CAsol-100	0.00054(6)	0.9	0.97	22
Ti-CAsol-125	0.00023(3)	1.5	0.99	
Ti-CAsol-150	0.0013(4)	2.0	0.93	

^a Values rounded to one decimal place.

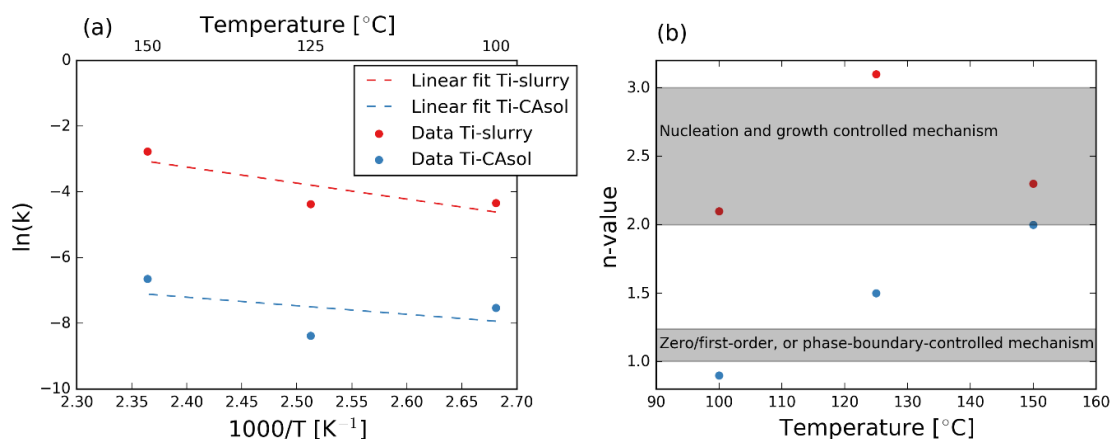


Figure 5. (a) Arrhenius plots for the Ti-slurry and Ti-CAsol with linear regression fits; (b) n -values plotted against temperature. Grey areas show physically meaningful values for n .

3.5. Phase Composition

All experiments yielded BT as the only or main phase. For Ti-CAsol-100, BT formed first followed by formation of BC, while BC formed before BT for the Ti-CAsol-EG. In both cases, BT was the main phase at the end of the experiment, with 88 and 95 wt % BT for Ti-CAsol-100 and Ti-CAsol-EG, respectively. No difference in the final results for the Ti-slurry experiments were observed with or without the mixing in ice bath. The only difference was the formation of BT immediately after adding KOH when not cooled, while BT formed during the experiments when mixing was done under cooling in an ice bath.

4. Discussion

Nanosized BT particles were successfully synthesized at a low temperature using two different titanium precursors and the reactions were followed in real time with in situ X-ray diffraction studies. The time resolved data demonstrated that, especially, the Ti-slurry precursor gives rapid BT formation compared to conventional autoclave synthesis (typical reaction times are in the range of hours and longer), but also compared with similar works [21,22]. The formation and growth of BT is finished in about 15 s for the Ti-slurry at 150 °C.

4.1. Kinetics

Comparing the results of the Ti-CAsol and the Ti-slurry shows that using citric acid to initially form a titanium-citric acid complex changes the reaction mechanisms. The reaction rate is higher for the Ti-slurry compared to the Ti-CAsol, which can be rationalized by an easier access to the Ti-atom. The n -values for the Ti-slurry indicate that it is the nucleation and growth that is the rate limiting step for all temperatures studied (see Figure 5b). On the other hand, the Ti-CAsol shows a nucleation and growth-controlled mechanism at 150 °C, but this changes into zero/first-order, or a phase boundary controlled mechanism, with decreasing temperature. In the works by Walton et al. [31], Eckert et al. [16], and Hertl [15], a n value of around 1 and a phase boundary mechanism as the rate limiting factor was reported, similar to the Ti-CAsol-100 in this work. The change to a nucleation and growth limiting mechanism, as seen in this work, with increasing temperature for the Ti-CAsol can be rationalized by an increased nucleation rate at higher temperatures. An increased nucleation rate is likely to be the reason the Ti-slurry behaving differently from the Ti-CAsol. We report here on different reaction mechanisms, depending on temperature and/or precursor, however, the final crystallite size is similar for all reactions (not including the experiments with surfactants). This could indicate that all reactions have a very high nucleation rate at the temperatures studied, which quickly depletes the precursors and limits further growth.

The activation energies calculated in this work are comparable to previously reported values of 105.5 [15], 43.2 [17], 55.1 [21], and 21 [32] kJ/mol. It should be noted here that direct comparison to the literature is difficult for kinetic studies, since these works cover different reaction conditions (temperatures, precursors, and solvents), which can, to some degree, explain the differences observed.

4.2. Refined Crystal Structure Parameters

It is clear from the refined values of size and strain that the peak broadening is mainly due to the size of the crystallites and not to any significant strain in the crystallites. Not many reports are found on Rietveld refinement of both size and strain on nanosized BT particles from wet chemical methods, since a wide Q -range is needed to differentiate between the two [33]. Size broadening is often assumed to be the dominant parameter and, thus, more often reported. Here, we show that this is the case by reporting small values of strain. BT, with a size of 30 nm, was prepared by Yan et al. from a high-gravity reactive precipitation method at 95 °C, with a refined strain value of 1.1×10^{-3} , which is comparable to the results in this work [34].

The lattice parameter evolution of BT for all experiments decreases initially before stabilization at around 4.05 Å, which is significantly higher than the bulk value for cubic BT at room temperature of 4.0094(2) Å [35] and 4.0126(2) Å at 150 °C [36]. The observed finite-size effect in lattice parameter is consistent with values observed in the literature of 4.03, 4.03, and 4.04 Å [21,22,34]. The large lattice parameter (4.05 Å compared to literature around 4.03–4.04 Å) seen in this work can be linked to the large disorder, as evident from the high B_{iso} values of titanium and barium. The values reported here (3–4 and 2–3 Å² at 150 °C for Ti and Ba, respectively) are higher than the values reported in similar works even at lower temperatures and similar crystallite sizes (2 and 1 Å² at 400 °C for Ti and Ba, respectively) [22]. This additional disorder can be the reason for the larger lattice parameter. The decreasing trend in B_{iso} for Ti in the Ti-slurry experiments with increasing temperature can also

explain the decrease in lattice parameter and strain observed. The difference between the strain and lattice parameters obtained for the Ti-slurry and Ti-CAsol experiments (values for Ti-CAsol are lower than of Ti-slurry) can be rationalized in the same way, with the difference in disorder (B_{iso} values of Ti-CAsol are lower than of Ti-slurry).

4.3. Effect of Surfactants

Almost a doubling of the crystallite size is observed when adding SDBS to the Ti-slurry, while a decrease is observed when adding EG. The differences observed for the lattice parameters is a direct effect of the different sizes, with the smaller sized Ti-slurry-EG giving a larger lattice parameter. The reaction rate seems to be unaffected by the presence of SDBS or EG. The main effect of the surfactants for the Ti-CAsol is that the presence of EG promotes the formation of BC, while only small changes are observed for the crystallite size and lattice parameter.

Hydrothermally synthesized KNbO_3 (KN) nanorods [37] and hierarchically nanostructured PbTiO_3 (PT) [38] have been reported when using SDBS as a surfactant (in combination with EG for PT). The results in this work do not suggest the formation of nanorods or hierarchical nanostructures, despite BT, KN, and PT all being perovskite oxides.

5. Conclusions

A thorough in situ X-ray diffraction investigation of a facile synthesis route of BT nanoparticles using two different titanium precursors was performed. Nanocrystalline BT (15 nm) forms within a few seconds or up to several hours, depending on the type of precursors and temperature. The relatively large lattice parameters (4.05 \AA) are linked to significant disorder in the material, as evident from the large values of ADP of titanium and barium ($3\text{--}4$ and $2\text{--}3 \text{ \AA}^2$ for Ti and Ba, respectively). Isotropic strain (1×10^{-3}) is shown to not be a significant contributor to the X-ray diffraction peak broadening. A kinetic study revealed that the two titanium precursors used behave similarly at high temperatures, but not at lower temperatures. This demonstrates the strength of in situ studies for understanding the nucleation and growth under hydrothermal conditions.

Supplementary Materials: The following are available online at <http://www.mdpi.com/2073-4352/8/6/253/s1>, Figure S1: Heating profiles for two different set-point temperatures (red (100°C) and green (150°C)). Blue data corresponds to 150°C , but with the capillary moved 0.5 mm closer to the heat blower compared to the green data showing the robustness of this setup; Figure S2: Last frames of experiments Ti-CAsol-150 and Ti-slurry-150 showing typical refinements, with red markers showing diffraction lines of BaTiO_3 at RT from ICDD card #01-074-4539. Refined values (R-values, lattice parameter, size, strain and atomic displacement parameters) are reported in Table S1; Figure S3: SEM images of Ti-CAsol-125 at two different magnifications, showing agglomerated spherical BaTiO_3 nanoparticles with a size $< 30 \text{ nm}$; Figure S4: Refined atomic displacement parameters for (a-b) Ti-slurry, and (c-d) Ti-CAsol experiments. (a) refined B_{iso} values for Ba; (b) refined B_{iso} values for Ti; (c) refined B_{iso} values for Ba; (d) refined B_{iso} values for Ti. Color-coding is as described in (a) for all panels; Figure S5: Normalized scale factor and fit to the Johnson-Mehl-Avrami equation for all samples used for the kinetic modeling; Table S1: Refined values (size, strain, lattice parameter, atomic displacement parameters for Ti and Ba and R-values) for the last frame from each experiment. Refinements were done using space group no. 221, $m\bar{3}m$, for BaTiO_3 .

Author Contributions: O.G.G., S.M.S., T.G. and M.-A.E. conceived and designed the experiments; O.G.G., A.B.B., S.L.S. and W.v.B. performed the in situ X-ray diffraction experiments; O.G.G. performed the experiments and analyzed the data; O.G.G., and M.-A.E. wrote the paper with inputs from all the authors.

Funding: This research was funded by The Research Council of Norway grant numbers 250403 and 245936/F50”.

Acknowledgments: Financial support from NTNU Norwegian University of Science and Technology and The Research Council of Norway under the Toppforsk program to the project (No 250403) “From Aqueous Solutions to oxide Thin films and hierarchical Structures” is gratefully acknowledged. The Research Council of Norway is acknowledged for the support to NTNU NanoLab through the Norwegian Micro and Nano-Fabrication Facility, NorFab, project number 245936/F50.

Conflicts of Interest: The authors declare no conflict of interest.

References

- Varghese, J.; Whatmore, R.W.; Holmes, J.D. Ferroelectric nanoparticles, wires and tubes: Synthesis, characterisation and applications. *J. Mater. Chem. C* **2013**, *1*, 2618–2638. [[CrossRef](#)]
- Villafuerte-Castrejon, M.E.; Moran, E.; Reyes-Montero, A.; Vivar-Ocampo, R.; Pena-Jimenez, J.A.; Rea-Lopez, S.O.; Pardo, L. Towards Lead-Free Piezoceramics: Facing a Synthesis Challenge. *Materials* **2016**, *9*, 27. [[CrossRef](#)] [[PubMed](#)]
- Shandilya, M.; Rai, R.; Singh, J. Review: Hydrothermal technology for smart materials. *Adv. Appl. Ceram.* **2016**, *115*, 354–376. [[CrossRef](#)]
- Gomes, M.A.; Lima, A.S.; Eguiluz, K.I.B.; Salazar-Banda, G.R. Wet chemical synthesis of rare earth-doped barium titanate nanoparticles. *J. Mater. Sci.* **2016**, *51*, 4709–4727. [[CrossRef](#)]
- Modeshia, D.R.; Walton, R.I. Solvothermal synthesis of perovskites and pyrochlores: Crystallisation of functional oxides under mild conditions. *Chem. Soc. Rev.* **2010**, *39*, 4303–4325. [[CrossRef](#)] [[PubMed](#)]
- Sun, W.; Pang, Y.; Li, J.; Ao, W. Particle Coarsening II: Growth Kinetics of Hydrothermal BaTiO₃. *Chem. Mater.* **2007**, *19*, 1772–1779. [[CrossRef](#)]
- Inada, M.; Enomoto, N.; Hayashi, K.; Hojo, J.; Komarneni, S. Facile synthesis of nanorods of tetragonal barium titanate using ethylene glycol. *Ceram. Int.* **2015**, *41*, 5581–5587. [[CrossRef](#)]
- Cai, W.; Rao, T.; Wang, A.; Hu, J.; Wang, J.; Zhong, J.; Xiang, W. A simple and controllable hydrothermal route for the synthesis of monodispersed cube-like barium titanate nanocrystals. *Ceram. Int.* **2015**, *41*, 4514–4522. [[CrossRef](#)]
- Dutta, P.K.; Gregg, J.R. Hydrothermal synthesis of tetragonal barium titanate (BaTiO₃). *Chem. Mater.* **1992**, *4*, 843–846. [[CrossRef](#)]
- Li, J.; Inukai, K.; Tsuruta, A.; Takahashi, Y.; Shin, W. Synthesis of highly disperse tetragonal BaTiO₃ nanoparticles with core-shell by a hydrothermal method. *J. Asian Ceram. Soc.* **2017**, *5*, 444–451. [[CrossRef](#)]
- Avrami, M. Kinetics of Phase Change. I General Theory. *J. Chem. Phys.* **1939**, *7*, 1103–1112. [[CrossRef](#)]
- Nørby, P.; Roelsgaard, M.; Søndergaard, M.; Iversen, B.B. Hydrothermal Synthesis of CoSb₂O₄: In Situ Powder X-ray Diffraction, Crystal Structure, and Electrochemical Properties. *Cryst. Growth Des.* **2016**, *16*, 834–841. [[CrossRef](#)]
- Andersen, H.L.; Jensen, K.M.Ø.; Tyrsted, C.; Bøjesen, E.D.; Christensen, M. Size and Size Distribution Control of γ -Fe₂O₃ Nanocrystallites: An in Situ Study. *Cryst. Growth Des.* **2014**, *14*, 1307–1313. [[CrossRef](#)]
- Eltzholtz, J.R.; Tyrsted, C.; Jensen, K.M.O.; Bremholm, M.; Christensen, M.; Becker-Christensen, J.; Iversen, B.B. Pulsed supercritical synthesis of anatase TiO₂ nanoparticles in a water-isopropanol mixture studied by in situ powder X-ray diffraction. *Nanoscale* **2013**, *5*, 2372–2378. [[CrossRef](#)] [[PubMed](#)]
- Hertl, W. Kinetics of Barium Titanate Synthesis. *J. Am. Ceram. Soc.* **1988**, *71*, 879–883. [[CrossRef](#)]
- Eckert, J.O.; Hung-Houston, C.C.; Gersten, B.L.; Lencka, M.M.; Riman, R.E. Kinetics and Mechanisms of Hydrothermal Synthesis of Barium Titanate. *J. Am. Ceram. Soc.* **1996**, *79*, 2929–2939. [[CrossRef](#)]
- Özen, M.; Mertens, M.; Snijders, F.; Cool, P. Hydrothermal synthesis and formation mechanism of tetragonal barium titanate in a highly concentrated alkaline solution. *Ceram. Int.* **2016**, *42*, 10967–10975. [[CrossRef](#)]
- Becker, J.; Bremholm, M.; Tyrsted, C.; Pauw, B.; Jensen, K.M.O.; Eltzholtz, J.; Christensen, M.; Iversen, B.B. Experimental setup for in situ X-ray SAXS/WAXS/PDF studies of the formation and growth of nanoparticles in near- and supercritical fluids. *J. Appl. Crystallogr.* **2010**, *43*, 729–736. [[CrossRef](#)]
- Sun, Y.; Ren, Y. In Situ Synchrotron X-ray Techniques for Real-Time Probing of Colloidal Nanoparticle Synthesis. *Part. Part. Syst. Charact.* **2013**, *30*, 399–419. [[CrossRef](#)]
- Jensen, K.M.; Tyrsted, C.; Bremholm, M.; Iversen, B.B. In situ studies of solvothermal synthesis of energy materials. *ChemSusChem* **2014**, *7*, 1594–1611. [[CrossRef](#)] [[PubMed](#)]
- Walton, R.I.; Millange, F.; Smith, R.I.; Hansen, T.C.; O'Hare, D. Real time observation of the hydrothermal crystallization of barium titanate using in situ neutron powder diffraction. *J. Am. Chem. Soc.* **2001**, *123*, 12547–12555. [[CrossRef](#)] [[PubMed](#)]
- Philippot, G.; Jensen, K.M.O.; Christensen, M.; Elissalde, C.; Maglione, M.; Iversen, B.B.; Aymonier, C. Coupling in situ synchrotron radiation with ex situ spectroscopy characterizations to study the formation of Ba_{1-x}Sr_xTiO₃ nanoparticles in supercritical fluids. *J. Supercrit. Fluids* **2014**, *87*, 111–117. [[CrossRef](#)]
- Dyadkin, V.; Pattison, P.; Dmitriev, V.; Chernyshov, D. A new multipurpose diffractometer PILATUS@SNBL. *J. Synchrotron Radiat.* **2016**, *23*, 825–829. [[CrossRef](#)] [[PubMed](#)]

24. Skjærvø, S.L.; Wells, K.H.; Sommer, S.; Vu, T.-D.; Tolchard, J.R.; van Beek, W.; Grande, T.; Iversen, B.B.; Einarsrud, M.-A. Rationalization of Hydrothermal Synthesis of NaNbO₃ by Rapid in Situ Time-Resolved Synchrotron X-ray Diffraction. *Cryst. Growth Des.* **2018**, *18*, 770–774. [[CrossRef](#)]
25. Dalod, A.R.M.; Grendal, O.G.; Skjærvø, S.L.; Inzani, K.; Selbach, S.M.; Henriksen, L.; van Beek, W.; Grande, T.; Einarsrud, M.-A. Controlling Oriented Attachment and in Situ Functionalization of TiO₂ Nanoparticles During Hydrothermal Synthesis with APTES. *J. Phys. Chem. C* **2017**, *121*, 11897–11906. [[CrossRef](#)]
26. Evans, J.S.O. Advanced Input Files & Parametric Quantitative Analysis Using Topas. *Mater. Sci. Forum* **2010**, *650*, 1–9. [[CrossRef](#)]
27. Thompson, P.; Cox, D.E.; Hastings, J.B. Rietveld refinement of Debye-Scherrer synchrotron X-ray data from Al₂O₃. *J. Appl. Crystallogr.* **1987**, *20*, 79–83. [[CrossRef](#)]
28. Dalod, A.R.M.; Henriksen, L.; Grande, T.; Einarsrud, M.-A. Functionalized TiO₂ nanoparticles by single-step hydrothermal synthesis: The role of the silane coupling agents. *Beilstein J. Nanotechnol.* **2017**, *8*, 304–312. [[CrossRef](#)] [[PubMed](#)]
29. Yoshiasa, A.; Nakatani, T.; Nakatsuka, A.; Okube, M.; Sugiyama, K.; Mashimo, T. High-temperature single-crystal X-ray diffraction study of tetragonal and cubic perovskite-type PbTiO₃ phases. *Acta Crystallogr. Sect. B* **2016**, *72*, 381–388. [[CrossRef](#)] [[PubMed](#)]
30. Peterson, K.M.; Heaney, P.J.; Post, J.E. A kinetic analysis of the transformation from akaganeite to hematite: An in situ time-resolved X-ray diffraction study. *Chem. Geol.* **2016**, *444*, 27–36. [[CrossRef](#)]
31. Walton, R.I.; Norquist, A.; Smith, R.I.; O'Hare, D. Recent results from the in situ study of hydrothermal crystallisations using time-resolved X-ray and neutron diffraction methods. *Faraday Discuss.* **2002**, *122*, 331–341. [[CrossRef](#)]
32. Ovramenko, N.A.; Shevts, L.I.; Ovcharenko, F.D.; Kornilovich, B.Y. Kinetics of Hydrothermal Synthesis of Barium Metatitanate. *Izv. Akad. Nauk SSSR Neorg. Mater.* **1979**, *15*, 1982–1985.
33. Balzar, D.; Audebrand, N.; Daymond, M.R.; Fitch, A.; Hewat, A.; Langford, J.I.; Le Bail, A.; Louer, D.; Masson, O.; McCowan, C.N.; et al. Size-strain line-broadening analysis of the ceria round-robin sample. *J. Appl. Crystallogr.* **2004**, *37*, 911–924. [[CrossRef](#)]
34. Yan, T.; Shen, Z.-G.; Zhang, W.-W.; Chen, J.-F. Size dependence on the ferroelectric transition of nanosized BaTiO₃ particles. *Mater. Chem. Phys.* **2006**, *98*, 450–455. [[CrossRef](#)]
35. Aoyagi, S.; Kuroiwa, Y.; Sawada, A.; Yamashita, I.; Atake, T. Composite Structure of BaTiO₃ Nanoparticle Investigated by SR X-ray Diffraction. *J. Phys. Soc. Jpn.* **2002**, *71*, 1218–1221. [[CrossRef](#)]
36. He, Y. Heat capacity, thermal conductivity, and thermal expansion of barium titanate-based ceramics. *Thermochim. Acta* **2004**, *419*, 135–141. [[CrossRef](#)]
37. Wang, G.Z.; Yu, Y.D.; Grande, T.; Einarsrud, M.A. Synthesis of KNbO₃ Nanorods by Hydrothermal Method. *J. Nanosci. Nanotechnol.* **2009**, *9*, 1465–1469. [[CrossRef](#)] [[PubMed](#)]
38. Wang, G.; Rørvik, P.M.; van Helvoort, A.T.J.; Holmestad, R.; Grande, T.; Einarsrud, M.-A. Self-Assembled Growth of PbTiO₃ Nanoparticles into Microspheres and Bur-like Structures. *Chem. Mater.* **2007**, *19*, 2213–2221. [[CrossRef](#)]

